Distribution Agreement

In presenting this thesis as a partial fulfillment of the requirements for a degree from Emory University, I hereby grant to Emory University and its agents the non-exclusive license to archive, make accessible, and display my thesis in whole or in part in all forms of media, now or hereafter now, including display on the World Wide Web. I understand that I may select some access restrictions as part of the online submission of this thesis. I retain all ownership rights to the copyright of the thesis. I also retain the right to use in future works (such as articles or books) all or part of this thesis.

Catharine Anderson April 12, 2022

Investigating Influenza Hemagglutinin Fusion Peptide Insertion into Model Membrane Liposomes with Fluorescence and FTIR Spectroscopy

by

Catharine Anderson

R. Brian Dyer
Adviser

Department of Chemistry

R. Brian Dyer

Adviser

Vincent Conticello

Committee Member

James Morey

Committee Member

2022

Investigating Influenza Hemagglutinin Fusion Peptide Insertion into Model Membrane Liposomes with Fluorescence and FTIR Spectroscopy

By

Catharine Anderson

R. Brian Dyer

Adviser

An abstract of
a thesis submitted to the Faculty of Emory College of Arts and Sciences
of Emory University in partial fulfillment
of the requirements of the degree of
Bachelor of Science with Honors

Department of Chemistry

2022

Abstract

Investigating Influenza Hemagglutinin Fusion Peptide Insertion into Model Membrane Liposomes with Fluorescence and FTIR Spectroscopy

By Catharine Anderson

The highly conserved first 23 residues of influenza hemagglutinin (HA), known as the fusion peptide (FP), are critical for fusion of the viral and endosomal membranes during viral infection. Even conservative substitutions in the FP have been shown to significantly alter the peptide's conformational ensemble and abolish fusogenicity. Equilibrium fluorescence and FTIR spectroscopy are used here to study the effects of different point mutations on fusion peptide insertion into vesicles. Insertion is initiated by heating DPPC (1,2-dipalmitoyl-sn-glycero-3-phosphocholine) lipid vesicles above the gel-to-liquid phase transition temperature of DPPC. In addition to the WT peptide, this study examines the variants G1V, W14A, G8A, and G16A. Each of these point mutations is expected to disrupt the tight helical hairpin structure of the WT FP. The G1V and W14A variants, which are expected to sample wide-angle open conformations, appear to insert more shallowly than WT or allow more water leakage into the membrane. The G8A and G16A variants, which are expected to sample acute-angle open conformations, appear to partially insert at lower temperatures than WT and disorder the membrane lipid tails to a greater extent. Fusion peptide insertion appears to be irreversible, most likely due to the disordering of the peptides and membrane environment at higher temperatures. With the equilibrium signals characterized, time-resolved temperature-jump fluorescence and FTIR spectroscopy could be used to

visualize the timescale of insertion for each fusion peptide variant. Resolving the temporal and spatial details of fusion peptide insertion could eventually enable the development of a universal influenza treatment.

Investigating Influenza Hemagglutinin Fusion Peptide Insertion into Model Membrane Liposomes with Fluorescence and FTIR Spectroscopy

By

Catharine Anderson

R. Brian Dyer

Adviser

A thesis submitted to the Faculty of Emory College of Arts and Sciences
of Emory University in partial fulfillment
of the requirements of the degree of
Bachelor of Science with Honors

Department of Chemistry

2022

Acknowledgements

I would like to thank Dr. Brian Dyer, my research advisor and honors thesis committee chair, for guiding me through my undergraduate research experience. His support and advice have made it possible for me to complete this honors thesis and be accepted to attend medical school after graduation.

I would also like to thank Dr. Vincent Conticello and Dr. James Morey for their willingness to serve as members of my committee and their interest in my research. In addition, I am thankful to all three of my committee members for being excellent professors who have taught some of the most enjoyable classes I have taken during my undergraduate years.

I am grateful to all past and current members of the Dyer lab for always being helpful and pleasant to work with. I would especially like to thank my graduate mentors Brooke Andrews and Alexia Prokopik, who dedicated so much of their time to teach me everything I know about lab techniques and research, in addition to giving me general advice and encouragement.

Finally, I am thankful for the love and support of my parents, older brother and sister-in-law, younger sister, and friends throughout my time in college.

Table of Contents

List of Figures

Chapter 1: Introduction to Hemagglutinin-Mediated Viral Membrane Fusion

1.1 Introduction

1.1.1 Influenza Hemagglutinin Structure and Role in Membrane Fusion

Fusion of the viral membrane with a target cell or endosomal membrane is a critical step in the viral life cycle. Upon fusion, viral contents are released into the cell, allowing subsequent replication and spread of the virus.[1] Although membrane fusion is thermodynamically favorable overall, it involves high-energy intermediate states that require coupling to protein dynamics in order to occur on the biological timescale.[2] Hemagglutinin (HA) is the homotrimeric, membrane-embedded fusion protein of the influenza virus.[3] Its precursor form, HA_0, is cleaved into two disulfide-linked units called HA_1 and HA_2 before incorporation into the membrane.[3] Each HA protein consists of three noncovalently associated HA_1/HA_2 subunits.[3] The protein is anchored in the membrane by the C-terminal transmembrane domain, which consists of three hydrophobic alpha helices, one from each monomer.[4] The globular HA_1 domain binds to the target cell's sialic acid receptors, while the HA_2 domain mediates membrane fusion.[3] HA_2 forms a rod-like coiled coil structure consisting of one alpha-helix from each monomer.[3] The fusion peptide (FP), a highly conserved ~20-25-residue segment that lies in the middle of the protein's peptide sequence in its precursor form, becomes the N-terminus of HA_2 after cleavage.[3] Its role is to insert into the target cell's membrane, helping to bring the two membranes into proximity and mediate fusion.[5] During fusion, the two membranes are thought to pass through a hemifusion intermediate in which only their outer leaflets mix together.[5] Once the inner leaflets mix together, a fusion pore is formed,[5] allowing the viral contents to empty out into the host cell. The process of membrane fusion is illustrated in Figure 1.1.

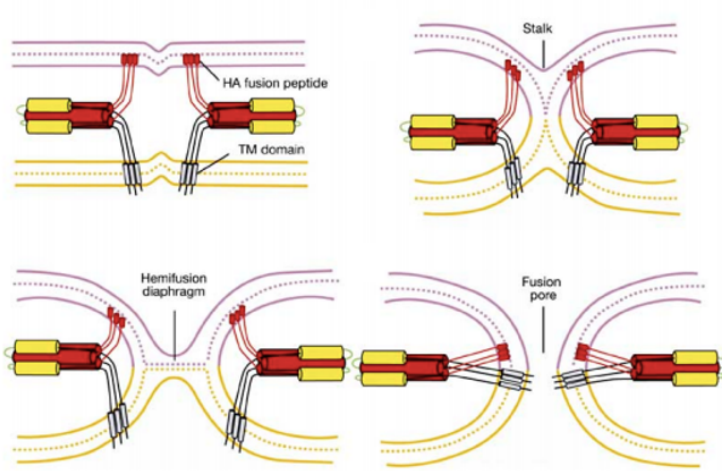

Figure 1.1. The spring-loaded model of hemagglutinin-mediated membrane fusion, passing through stalk and hemifusion intermediates before the fusion pore is formed. Reprinted from reference 5. Copyright 2009.

After binding to the cell's sialic acid receptors, the influenza virus is endocytosed. HA undergoes an activating conformational change triggered by the acidification of the late endosome to pH ~4-5 in an attempt to degrade its contents.[3] X-ray crystallography has revealed the structure of the HA ectodomain in its precursor form, in its cleaved form at neutral pH, and in its cleaved form at low pH.[6,7,8] The pH-triggered conformational change seems to involve the dissociation of the HA1 subunits, extension of the fusion peptides toward the target membrane, and folding of the fusion peptides back towards the transmembrane domain in order to bring the two membranes into proximity.[9] The precise spatial and temporal details of these conformational changes are still under investigation. Multiple models have been suggested to describe the pH-triggered conformational changes of HA.

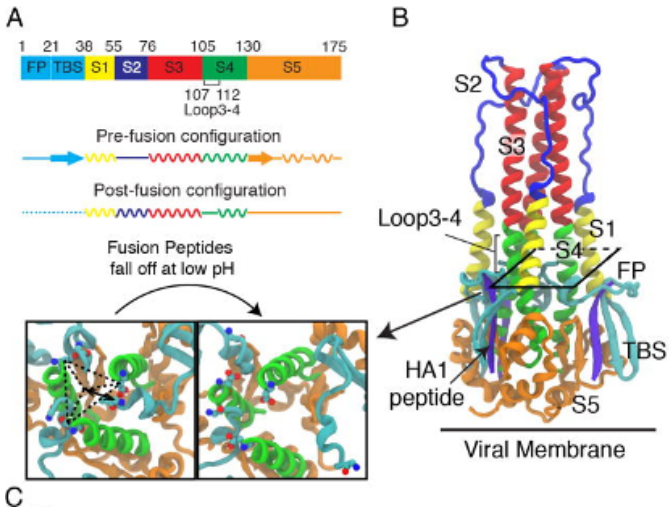

Figure 1.2. (A) Primary and secondary structure of the HA2 domain of hemagglutinin. (B) Quaternary structure of HA2 in its cleaved form at neutral pH, before the conformational change that allows FP insertion into the endosomal membrane. (C) Illustration of the conformational change that occurs at low pH. Reprinted with permission from reference 10. Copyright 2016 American Chemical Society.

The most popular model, often called the “spring-loaded” mechanism, posits that HA2 is caught in a metastable conformation sterically constrained by the presence of the HA1 at neutral pH.[3] After dissociation of HA1 at low pH, HA2 can undergo a conformational loop-to-helix transition that extends the coiled-coil, presenting all three fusion peptides to the target membrane for insertion,[3] as illustrated in Figure 1.1. Another model proposes the existence of a symmetry-broken intermediate, which causes the fusion peptides to insert asymmetrically into both the target and viral membranes.[10] The extension of the coiled coil occurs after fusion peptide insertion in this model.[10] In both models, the two membranes are brought closer together by the

melting of a domain near the C-terminus of HA2 which packs antiparallel into the central coiled coil, bringing the fusion peptides and transmembrane domain to the same end.[9]

1.1.2 Wild Type Fusion Peptide Structure

The purpose of this study is to investigate the role of the fusion peptide in driving membrane fusion. The structure of the FP has not been resolved crystallographically because of its poor solubility, but it has been explored through other techniques such as NMR.[5,14] It appears to fold into a helical hairpin structure at neutral pH (shown in Figure 1.3), while more open V-shaped helical conformations become transiently accessible at low pH.[14] The mechanism by which FP insertion promotes membrane fusion is still unclear, but experiments have revealed that fusogenicity is related to insertion depth and angle, degree of helicity, membrane binding affinity, effects on membrane order and curvature, and dehydration of the membrane surface.[11,12] Many experiments have probed FP function by mutating critical residues such as the N-terminal glycine or the residues in the kink region.[13]

1.1.3 Fusion Peptide Variants Structure

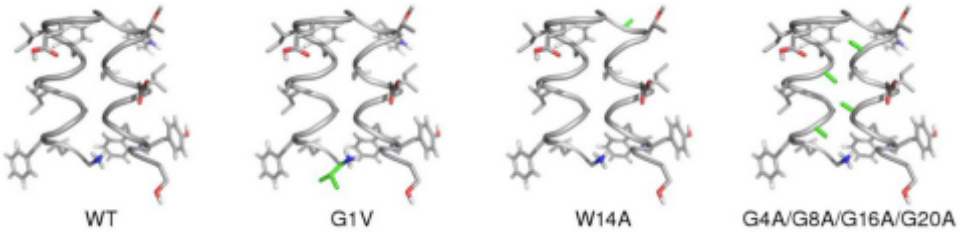

Figure 1.3. Helical hairpin structure of the hemagglutinin fusion peptide. Locations of point mutations are shown by the residues in green. Reprinted from reference 2. Copyright 2016.

In this study, four FP variants with point mutations are investigated in addition to the wild type (WT) FP: G1V, W14A, G8A, and G16A. Computational modeling predicts all of these mutants to sample open conformations to a greater extent than WT, with varying angles.[14,16,17] The Gly-1 residue of the FP has been demonstrated to be important in establishing a charge-dipole interaction between the N-terminal amide group and the dipole associated with the other end of the FP helix, which stabilizes the helical hairpin structure.[15] Mutating the N-terminal glycine is predicted to cause the G1V FP to adopt a nearly linear open structure as shown in Figure 1.4.[16]

Trp-14 of the FP is situated in the kink region.[2] Mutating it to alanine is expected to make the kink region more flexible, also disrupting the helical hairpin structure and causing the W14A FP to adopt a more open “boomerang” conformation as shown in Figure 1.4.[17]

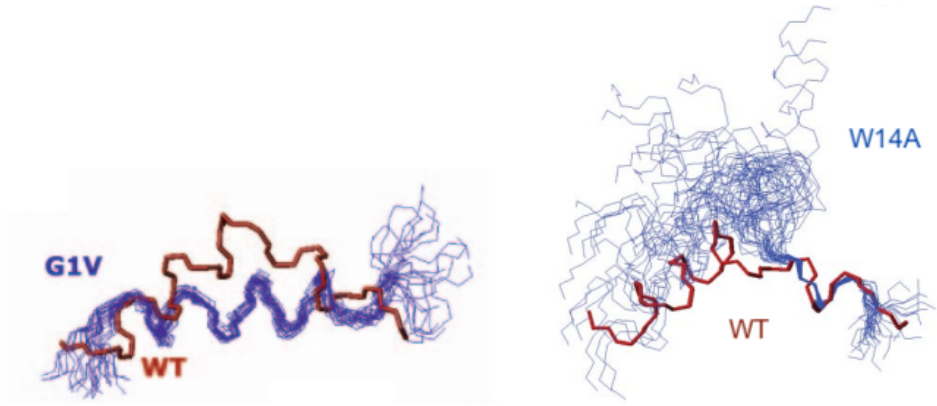

Figure 1.4. *Left*: Linear conformation of G1V FP. Reprinted from reference 16. Copyright 2005. *Right*: “Boomerang” conformation of W14A FP. Reprinted from reference 17. Copyright 2006.

There are four glycine residues in positions 4, 8 ,16, and 20 of the FP thought to be involved in a “glycine zipper” that holds the two helical segments together in the helical

hairpin structure.[2] Mutating these glycine residues is expected to destabilize the helical hairpin, and position 8 has been shown to be especially sensitive to mutations.[18] The G8A variant likely adopts two open conformations, one with a wide angle similar to W14A and one with an acute angle similar to the open conformation of the WT FP at low pH,[14] as shown in Figure 1.5. The structure of the G16A mutant has not been modelled, but since G16 occupies a similar position to G8 as its partner in the glycine zipper, the structure of G16A may be similar to G8A.

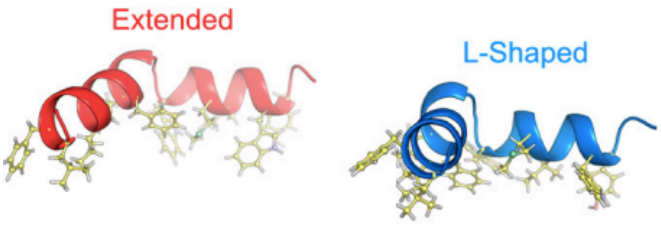

Figure 1.5. Extended and L-shaped open structures of G8A FP. Reprinted from reference 14. Copyright 2012.

By studying point mutations of the FP, the importance of the WT FP's interactions with the endosomal membrane to drive membrane fusion can be better understood. Even conservative mutations in the FP sequence can completely abolish fusion activity, raising the possibility that a treatment targeting the influenza fusion peptide could eventually be developed which would be effective against all serotypes and could not be evaded by viral mutation.[14] Understanding the mechanism by which fusion peptide insertion promotes membrane fusion in conjunction with the rest of the HA protein is a critical first step in this direction.

1.2 Conclusions and aims

The dynamics of influenza hemagglutinin fusion peptide insertion into the endosomal membrane have yet to be characterized. In this study, fluorescence and Fourier Transform Infrared (FTIR) spectroscopy are both used to observe insertion of the FP into model membrane liposomes. Fluorescence emission can be used to detect changes in the environment around the intrinsic tryptophan residues of the FP, while FTIR spectroscopy tracks changes in the environment around the peptide amide groups, lipid hydrophobic tail groups, and lipid headgroups. In order to investigate the importance of the highly conserved FP primary sequence, experiments are performed using the G1V, G8A, G18A, and W14A variants of the FP in addition to the WT.

1.3 References

1. Ryu, W.-S. Virus life cycle. https://www.ncbi.nlm.nih.gov/pmc/articles/PMC7158286/ (accessed Mar 18, 2022).
2. Lousa, D.; Pinto, A. R.; Victor, B. L.; Laio, A.; Veiga, A. S.; Castanho, M. A.; Soares, C. M. Fusing Simulation and Experiment: The Effect of Mutations on the Structure and Activity of the Influenza Fusion Peptide. *Scientific Reports* **2016**, *6* (1).
3. Boonstra, S.; Blijleven, J. S.; Roos, W. H.; Onck, P. R.; van der Giessen, E.; van Oijen, A. M. Hemagglutinin-Mediated Membrane Fusion: A Biophysical Perspective. *Annual Review of Biophysics* **2018**, *47* (1), 153–173.
4. Tatulian, S. A.; Tamm, L. K. Secondary Structure, Orientation, Oligomerization, and Lipid Interactions of the Transmembrane Domain of Influenza Hemagglutinin. *Biochemistry* **1999**, *39* (3), 496–507.

5. Cross, K.; Langley, W.; Russell, R.; Skehel, J.; Steinhauer, D. Composition and Functions of the Influenza Fusion Peptide. *Protein & Peptide Letters* **2009**, *16* (7), 766–778.
6. Chen, J.; Lee, K. H.; Steinhauer, D. A.; Stevens, D. J.; Skehel, J. J.; Wiley, D. C. Structure of the Hemagglutinin Precursor Cleavage Site, a Determinant of Influenza Pathogenicity and the Origin of the Labile Conformation. *Cell* **1998**, *95* (3), 409–417.
7. Wilson, I. A.; Skehel, J. J.; Wiley, D. C. Structure of the Haemagglutinin Membrane Glycoprotein of Influenza Virus at 3 Å Resolution. *Nature* **1981**, *289* (5796), 366–373.
8. Chen, J.; Skehel, J. J.; Wiley, D. C. N- And C-Terminal Residues Combine in the Fusion-Ph Influenza Hemagglutinin Ha 2 Subunit to Form an N Cap That Terminates the Triple-Stranded Coiled Coil. *Proceedings of the National Academy of Sciences* **1999**, *96* (16), 8967–8972.
9. Borrego-Diaz, E.; Peeples, M. E.; Markosyan, R. M.; Melikyan, G. B.; Cohen, F. S. Completion of Trimeric Hairpin Formation of Influenza Virus Hemagglutinin Promotes Fusion Pore Opening and Enlargement. *Virology* **2003**, *316* (2), 234–244.
10. Lin, X.; Noel, J. K.; Wang, Q.; Ma, J.; Onuchic, J. N. Lowered Ph Leads to Fusion Peptide Release and a Highly Dynamic Intermediate of Influenza Hemagglutinin. *The Journal of Physical Chemistry B* **2016**, *120* (36), 9654–9660.
11. Wu, C.-W.; Cheng, S.-F.; Huang, W.-N.; Trivedi, V. D.; Veeramuthu, B.; Assen B, K.; Wu, W.-G.; Chang, D.-K. Effects of Alterations of the Amino-Terminal Glycine of Influenza Hemagglutinin Fusion Peptide on Its Structure, Organization and

Membrane Interactions. *Biochimica et Biophysica Acta (BBA) - Biomembranes* **2003**, *1612* (1), 41–51.

12. Chakraborty, H.; Tarafdar, P. K.; Klapper, D. G.; Lentz, B. R. Wild-Type and Mutant Hemagglutinin Fusion Peptides Alter Bilayer Structure as Well as Kinetics and Activation Thermodynamics of Stalk and Pore Formation Differently: Mechanistic Implications. *Biophysical Journal* **2013**, *105* (11), 2495–2506.
13. Worch, R. Structural Biology of the Influenza Virus Fusion Peptide. *Acta Biochimica Polonica* **2014**, *61* (3).
14. Lorieau, J. L.; Louis, J. M.; Schwieters, C. D.; Bax, A. PH-Triggered, Activated-State Conformations of the Influenza Hemagglutinin Fusion Peptide Revealed by NMR. *Proceedings of the National Academy of Sciences* **2012**, *109* (49), 19994–19999.
15. Lorieau, J. L.; Louis, J. M.; Bax, A. Helical Hairpin Structure of Influenza Hemagglutinin Fusion Peptide Stabilized by Charge−Dipole Interactions between the N-Terminal Amino Group and the Second Helix. *Journal of the American Chemical Society* **2011**, *133* (9), 2824–2827.
16. Li, Y.; Han, X.; Lai, A. L.; Bushweller, J. H.; Cafiso, D. S.; Tamm, L. K. Membrane Structures of the Hemifusion-Inducing Fusion Peptide Mutant G1S and the Fusion-Blocking Mutant G1V of Influenza Virus Hemagglutinin suggest a Mechanism for Pore Opening in Membrane fusion. *Journal of Virology* **2005**, *79* (18), 12065–12076.
17. Lai, A. L.; Park, H.; White, J. M.; Tamm, L. K. Fusion Peptide of Influenza Hemagglutinin Requires a Fixed Angle Boomerang Structure for Activity. *Journal of Biological Chemistry* **2006**, *281* (9), 5760–5770.

18. Wu, C.-W.; Cheng, S.-F.; Huang, W.-N.; Trivedi, V. D.; Veeramuthu, B.; Assen B, K.; Wu, W.-G.; Chang, D.-K. Effects of Alterations of the Amino-Terminal Glycine of Influenza Hemagglutinin Fusion Peptide on Its Structure, Organization and Membrane Interactions. *Biochimica et Biophysica Acta (BBA) - Biomembranes* **2003**, *1612* (1), 41–51.

Chapter 2: Characterization of Fusion Peptide Insertion into Model Membrane Liposomes with Fluorescence Spectroscopy

2.1 Introduction

Equilibrium fluorescence experiments were performed in order to establish changes in the environment surrounding the intrinsic tryptophan residues of the FP, which occupy positions 14 and 21, as it inserts into model membrane liposomes. Fluorescence emission undergoes a blue-shift and increase in intensity when tryptophan enters a more hydrophobic environment, such as a cell membrane.[1]

DPPC (1,2-dipalmitoyl-sn-glycero-3-phosphocholine) large unilamellar vesicles (LUVs) were used as model membrane liposomes. DPPC has a melting temperature of 41° C, at which it transitions from the gel to the fluid phase, with the presence of a comparatively transient ripple phase in between[2] as illustrated in Figure 2.1. The gel phase at lower temperatures is characterized by the rigid packing of hydrophobic lipid tails in an all-anti conformation, preventing fusion peptide insertion.[2] The fluid phase at higher temperatures is characterized by greater conformational entropy of the hydrophobic lipid tails, allowing gauche conformations, which prevents the tails from packing as tightly.[3] The fusion peptide, which is associated with the membrane surface below the T_m,[4] is therefore able to insert into the fluid membrane above the T_m.

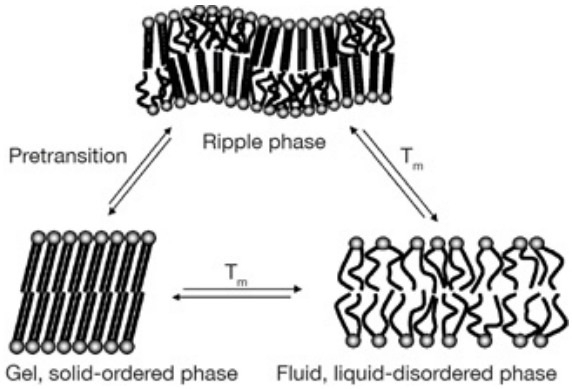

Figure 2.1. Temperature-dependent membrane phase transitions. Reprinted from reference 3. Copyright 2009.

Insertion is initiated in these equilibrium fluorescence experiments by raising the temperature of a solution of FP and DPPC LUVs above 41° C. The solution is acidic (pH = 4.5) since these are the conditions under which FP insertion is triggered biologically in the endosome.

2.2 Materials and Methods

2.1.1 Model Membrane Liposome Preparation

DPPC lipids were purchased from Avanti Polar Lipids, Inc. in chloroform. To prepare lipid cakes, the lipids in chloroform were aliquoted into 2 mL glass vials, and the chloroform was evaporated off with an N_2 gas stream. The vials were flash frozen with liquid N_2, placed on a lyophilizer overnight, and stored in a -20° C freezer before using. Directly before performing the fluorescence experiment, the lipid cakes were hydrated with 20 mM acetate buffer at pH 4.5 and subjected to 5 rounds of freezing and thawing on a hot plate at 55° C (above the T_m = 41° C of DPPC). To prepare large unilamellar vesicles (LUVs), the lipids were extruded 15 times on a hot plate at 55° C using an extruder from Avanti Polar Lipids, Inc. The size of the DPPC LUVs was verified via dynamic light scattering (DLS).

2.1.2 Fusion Peptide Preparation

Standard Fmoc solid phase synthesis on a rink amide resin was used to synthesis the H3 serotype of hemagglutinin fusion peptide, which has the sequence GLFGAIAGFIEGGWTGMIDGWYG-[GDGKKKK]. The G1V, W14A, G8A, and G16A FPs had sequences with the indicated point mutations. The instrument used for this synthesis was an acid-coupling CEM Liberty 1 peptide synthesizer (CEM Matthew, NC).

Fmoc-protected amino acids were purchased from AnaSpec Inc. (Fremont, CA). Following synthesis, HPLC was used to purify the solubility-tagged FP on a reverse phase C18 column (Phenomenex, Torrance, CA), with a linear gradient of water to acetonitrile and 0.1% TFA. The masses of the purified peptides were confirmed using MALDI spectrometry.

2.1.3 Fluorescence Emission

A Dual-FL spectrophotometer (Horiba Scientific, Edison, NJ) was used to collect equilibrium fluorescence data. In each experiment, the FP variant being studied was dissolved in DI water and mixed with the DPPC LUVs, resulting in a 1:50 peptide:lipid molar ratio with a total volume of 1 mL (50 μM FP, 25 mM LUVs). The mixture was kept on ice to prevent the FP from inserting prior to the experiment. Beginning at 20° C, the sample was heated to 70° C by 1° increments. At each temperature point, the sample was excited at 290 nm, and resulting fluorescence intensity was obtained by integrating the tryptophan emission peak between 324 and 356 nm. The following instrument parameters were used: 0.4 second integration time, 100 accumulations, total range of 285-550 nm, 3 nm excitation and emission slit width.

Corrected fluorescence intensity for each experiment was calculated by integrating the area under the fluorescence curve between 324 and 356 nm, normalizing to the fluorescence intensity at 20° C, and subtracting the normalized temperature-dependent fluorescence intensity of free tryptophan.

2.2 Results and Discussion

2.3.1 FP Insertion Melt Experiments

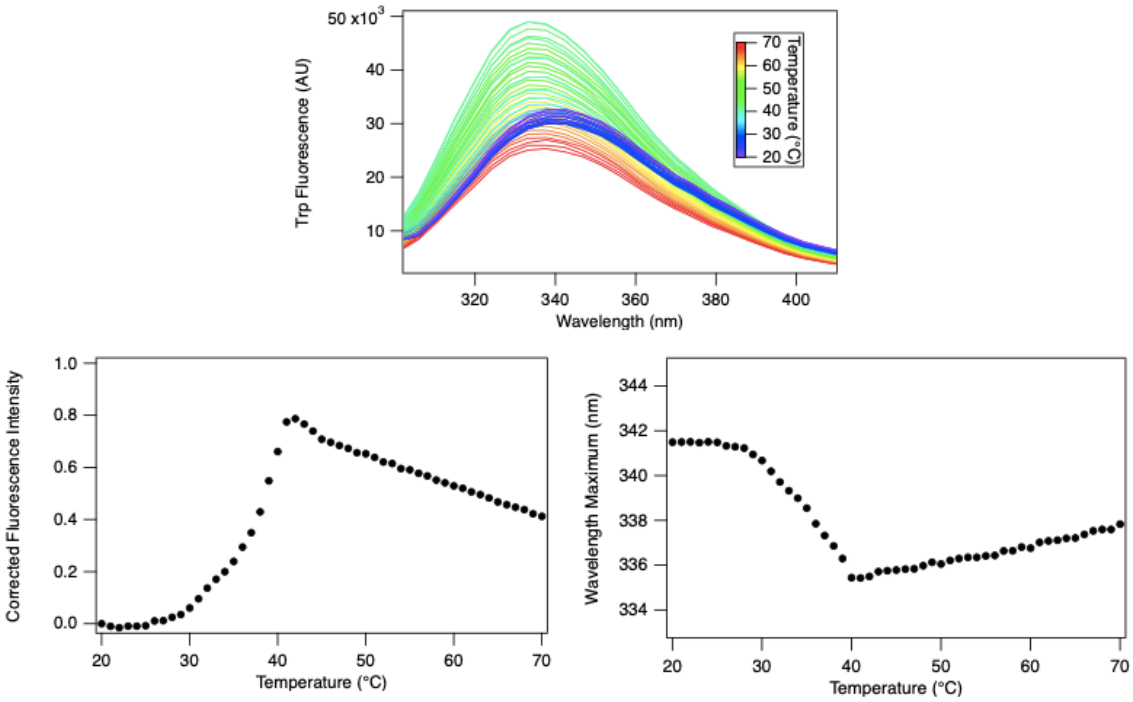

Figure 2.2. *Top*: Temperature-dependent fluorescence emission spectra of WT FP and DPPC LUVs in a 1:50 molar ratio heated from 20° to 70° C. *Bottom left*: Change in fluorescence emission intensity vs temperature, corrected for the temperature-dependence of tryptophan fluorescence. *Bottom right*: Change in wavelength maximum vs temperature; total shift in wavelength of 341.5 – 335.5 nm.

The WT FP (Figure 2.2) displays an increase in fluorescence intensity and a blue shift in wavelength emission maximum as the melting temperature of DPPC (T_m = 41° C) is approached. Both these trends are indicative of the peptide entering a more hydrophobic environment as it inserts into the membrane. All other FP variants (Figures

2.2-2.5) display the same increase in fluorescence intensity and shift to a lower wavelength before 41° C, but with slight differences resulting from their disrupted conformations. Examining these differences provides information about how these disrupted conformations affect FP insertion into the model membranes.

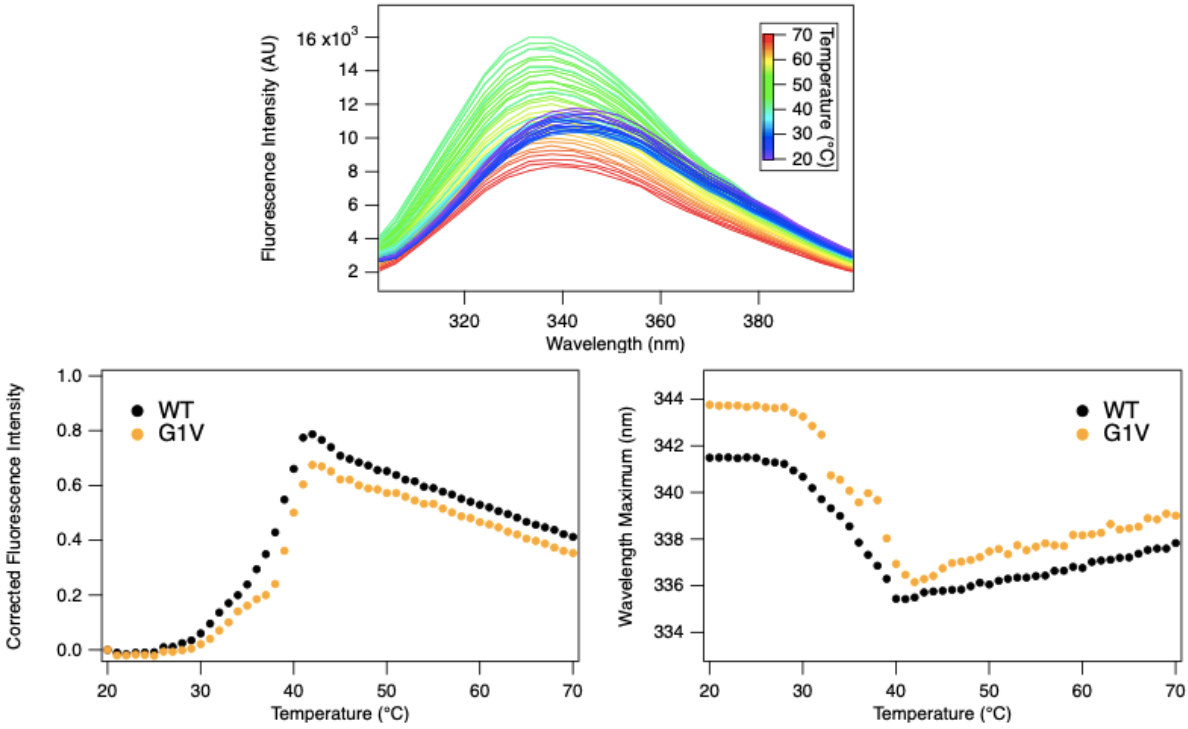

Figure 2.3. *Top*: Temperature-dependent fluorescence emission spectra of G1V FP and DPPC LUVs in a 1:50 molar ratio heated from 20° to 70° C. *Bottom left*: Change in fluorescence emission intensity vs temperature. *Bottom right*: Change in wavelength maximum vs temperature; total shift in wavelength of 344 – 336 nm.

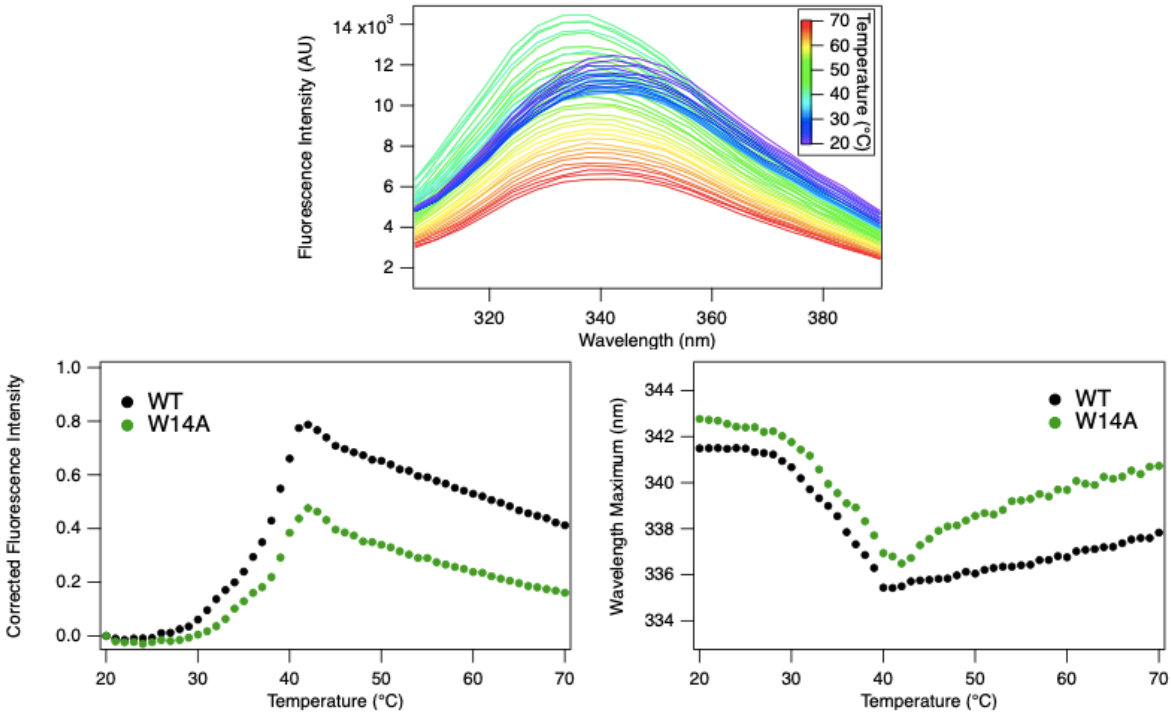

Figure 2.4. *Top*: Temperature-dependent fluorescence emission spectra of W14A FP and DPPC LUVs in a 1:50 molar ratio heated from 20° to 70° C. *Bottom left*: Change in fluorescence emission intensity vs temperature. *Bottom right*: Change in wavelength maximum vs temperature; total shift in wavelength of 343 – 336 nm.

The fluorescence peaks of the G1V (Figure 2.3) and W14A (Figure 2.4) variants begin at higher wavelengths than WT at 20° C. This could be a result of the G1V and W14A tryptophan residues being more water-exposed due to their altered conformations, or the WT FP partially inserting prior to the experiment to a greater extent than G1V and W14A. G1V and W14A do not show as great of an increase in fluorescence intensity as WT, indicating that they insert more shallowly or allow water leakage into the membrane more than WT. It should be noted that Trp-14 is mutated in

the W14A FP, and therefore Figure 2.4 only reflects changes in the environment around Trp-21, which is at the C-terminus of the FP. Since the FP inserts N-terminus first, this likely partially accounts for the smaller signal changes, although it has been reported elsewhere that W14A inserts more shallowly than WT.[5]

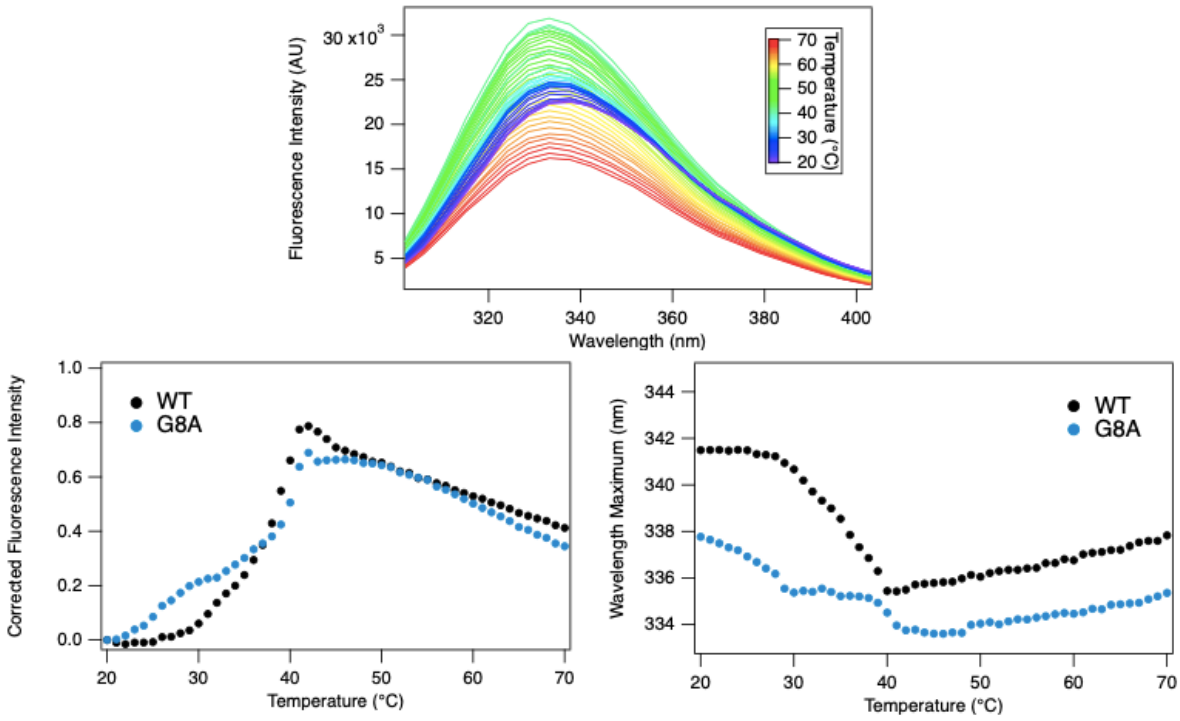

Figure 2.5. *Top*: Temperature-dependent fluorescence emission spectra of G8A FP and DPPC LUVs in a 1:50 molar ratio heated from 20° to 70° C. *Bottom left*: Change in fluorescence emission intensity vs temperature. *Bottom right*: Change in wavelength maximum vs temperature; total shift in wavelength of 338 – 333.5 nm.

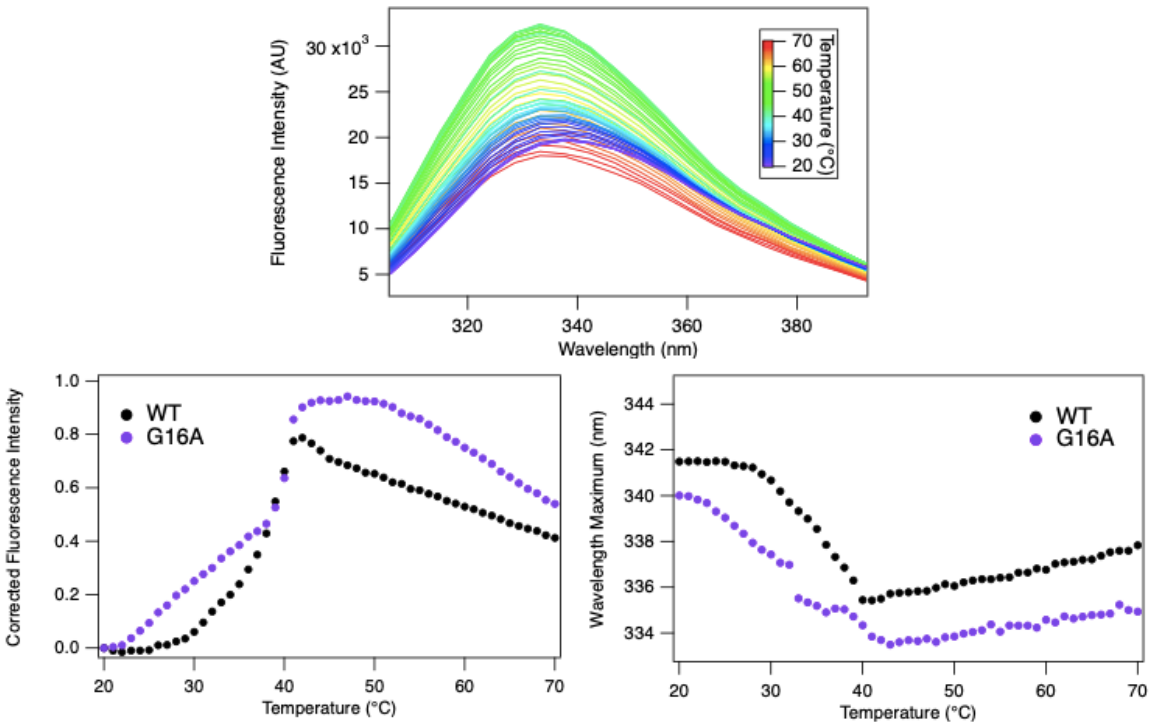

Figure 2.6. *Top*: Temperature-dependent fluorescence emission spectra of G16A FP and DPPC LUVs in a 1:50 molar ratio heated from 20° to 70° C. *Bottom left*: Change in fluorescence emission intensity vs temperature. *Bottom right*: Change in wavelength maximum vs temperature; total shift in wavelength of 340 – 333.5 nm.

The fluorescence peaks of the G8A (Figure 2.5) and G16A (Figure 2.6) variants, in contrast, begin at lower wavelengths than WT FP. This might indicate that the G8A and G16A variants have partially inserted prior to the experiment to a greater extent than WT. G8A shows a smaller increase in fluorescence intensity than WT, possibly because it has already partially inserted. G16A shows a slightly greater increase in fluorescence intensity despite likely having partially inserted at lower temperatures than WT, indicating that it inserts more deeply or excludes water from the membrane better than

WT. Both variants display insertion during the ripple phase prior to the DPPC T_m. The combination of the acute-angle open conformations sampled by G8A and G16A and the membrane disturbances present in the ripple phase likely allow for this pre-T_m insertion.

After 41° C, all FP variants display a decrease in fluorescence and a red shift in wavelength emission maximum. This is generally indicative of the peptides entering a more hydrophilic environment. The peptides could be aggregating, exiting the membrane, or being hydrated by water leakage into the membrane. The FTIR experiments in Chapter 3 were performed in order to determine which of these events is occurring at higher temperatures.

2.3.2 FP Insertion Reversibility Experiments

Insertion appears to be irreversible according to the data in Figure 2.7. After cooling the WT FP and DPPC LUVs mixture back to 20° C from 70° C, the fluorescence intensity and wavelength do not return to baseline. Only small changes are observed in fluorescence intensity and emission maximum upon cooling. Similar trends in reversibility were observed for all variants, not shown here.

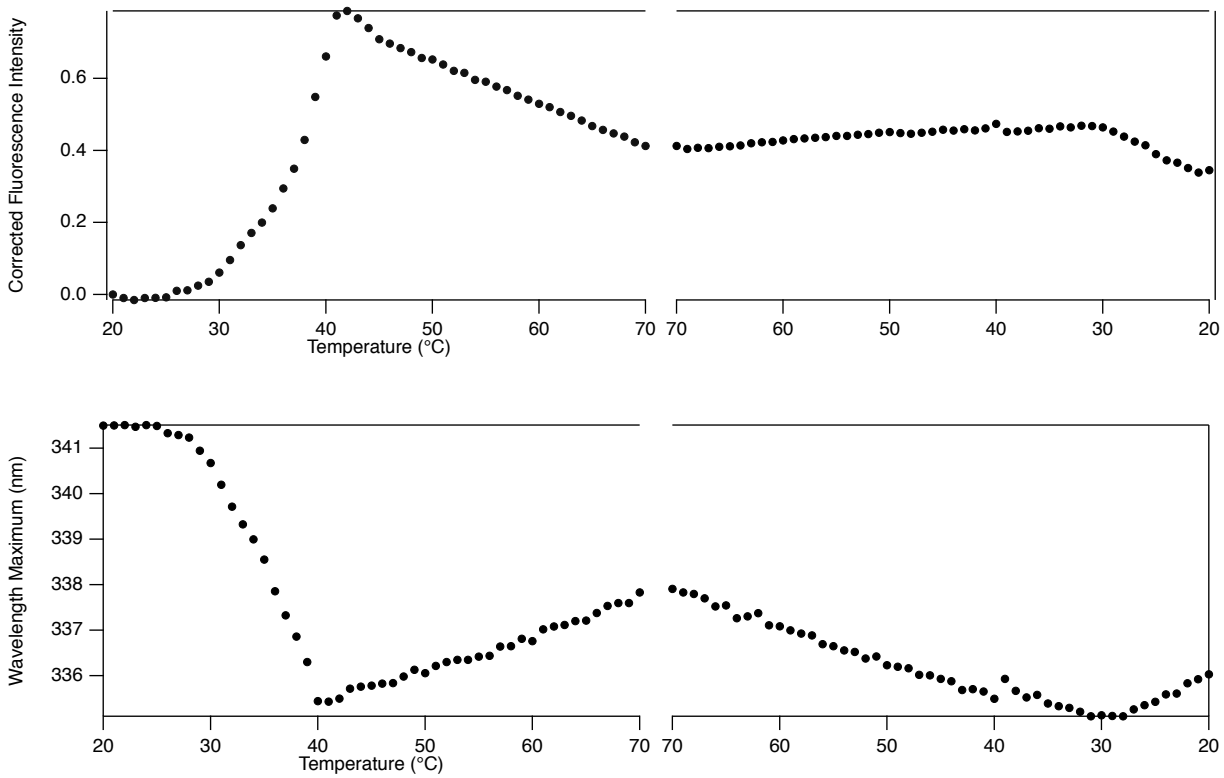

Figure 2.7. *Top:* Temperature-dependent fluorescence emission of WT FP and DPPC LUVs in a 1:50 molar ratio cooled from 70° to 20° C. *Top*: Change in fluorescence emission intensity vs temperature, corrected for the temperature-dependence of tryptophan fluorescence. *Bottom*: Change in wavelength maximum vs temperature.

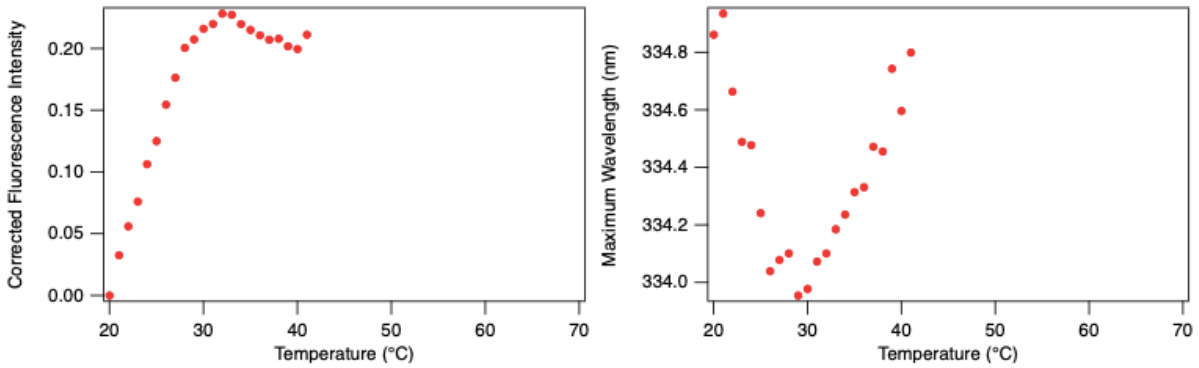

Figure 2.8. Temperature-dependent fluorescence emission of WT FP and DPPC LUVs in a 1:50 molar ratio, cooled from 41° to 20° C. *Left*: Change in fluorescence emission intensity vs temperature, corrected for the temperature-dependence of tryptophan fluorescence. *Right*: Change in wavelength maximum vs temperature; total shift in wavelength of 334.5– 334 nm.

The WT fluorescence melt was repeated, stopped at T_m = 41° C, and cooled back to 20° C to see if this would have any effect on the reversibility of insertion. Figure 2.8 shows the fluorescence change and wavelength shift upon cooling, which look very similar to that observed after cooling from 70° C. This indicates that the insertion event occurring at 41° C is itself irreversible, and that irreversibility is not due to an event occurring only at higher temperatures above the melting point, such as aggregation.

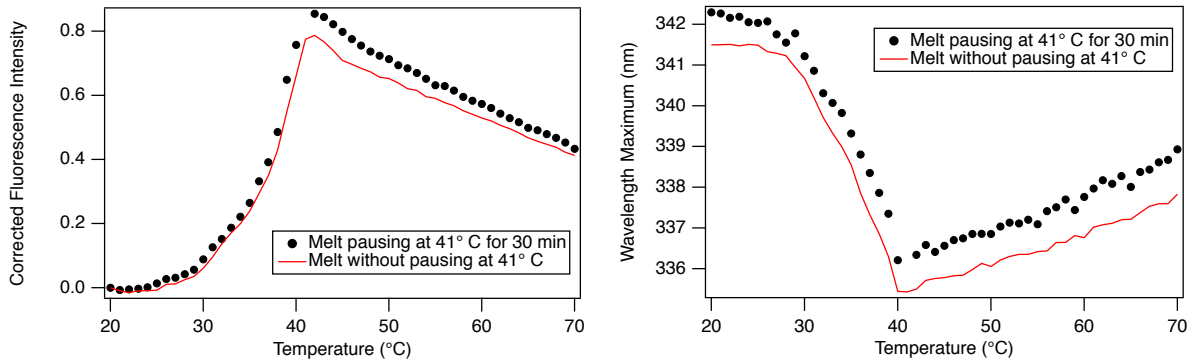

Figure 2.9. Temperature-dependent fluorescence emission of WT FP and DPPC LUVs in a 1:50 molar ratio, heated from 20° to 41° C, held at 41° C for 30 minutes, and then heated from 41° to 70° C. *Left*: Change in fluorescence emission intensity vs temperature, corrected for the temperature-dependence of tryptophan fluorescence. *Right*: Change in wavelength maximum vs temperature.

When the WT fluorescence melt was repeated and paused at 41° C for 30 minutes before continuing to 70° C, no significant change in fluorescence intensity or emission maximum was observed during the pause at 41° C, as shown in Figure 2.9. Whatever causes the fluorescence increase and red shift after 41° C is certainly temperature dependent. This would be an unexpected result if aggregation was the process causing FP insertion to be irreversible.

Overall, it remains unclear from these data whether the FP is aggregating, exiting the membrane, or becoming more solvent accessible at higher temperatures. However, the data presented in Chapter 3 provide evidence in agreement with Figures 2.8 and 2.9 that aggregation is not the reason for the observed irreversibility of insertion.

2.3 References

1. Vivian, J. T.; Callis, P. R. Mechanisms of Tryptophan Fluorescence Shifts in Proteins. *Biophysical Journal* **2001**, *80* (5), 2093–2109.
2. Nagarajan, S.; Schuler, E. E.; Ma, K.; Kindt, J. T.; Dyer, R. B. Dynamics of the Gel to Fluid Phase Transformation in Unilamellar DPPC Vesicles. *The Journal of Physical Chemistry B* **2012**, *116* (46), 13749–13756.
3. Eeman, M.; Deleu, M. From Biological Membranes to Biomimetic Model Membranes. *Biotechnologie, Agronomie, Société et Environnement/Biotechnology, Agronomy, Society and Environment* **2009**, *14* (4).
4. Lousa, D.; Pinto, A. R.; Victor, B. L.; Laio, A.; Veiga, A. S.; Castanho, M. A.; Soares, C. M. Fusing Simulation and Experiment: The Effect of Mutations on the Structure and Activity of the Influenza Fusion Peptide. *Scientific Reports* **2016**, *6* (1).
5. Lai, A. L.; Park, H.; White, J. M.; Tamm, L. K. Fusion Peptide of Influenza Hemagglutinin Requires a Fixed Angle Boomerang Structure for Activity. *Journal of Biological Chemistry* **2006**, *281* (9), 5760–5770.

Chapter 3: Characterization of Fusion Peptide Insertion into Model Membrane Liposomes with FTIR Spectroscopy

3.1 Introduction

Equilibrium FTIR experiments were performed in order to establish changes in the environments surrounding the FP backbone amide groups (~1600-1720 cm^{-1}),[1] DPPC hydrophobic lipid tails (~1680-1780 cm^{-1}),[2] and DPPC headgroup ester carbonyls (~2980-2820 cm^{-1})[3] during FP insertion into model membrane liposomes.

DPPC small unilamellar vesicles (SUVs) were used as model membrane liposomes. To trigger insertion, samples containing the FP and DPPC SUVs were heated above 41° C, the melting temperature of DPPC, as explained in section 2.1. There are three regions of the FTIR spectrum that can be monitored as FP insertion occurs. The amide region of the difference spectrum provides information about whether the alpha-helix is solvated or buried, and whether it unfolds from the alpha-helical conformation. The C-H lipid tail region shows the melting of the membrane and is sensitive to disordering of the lipid tails. Finally, previous studies[3] have used FTIR to look at the percentage of DPPC headgroup carbonyls that are hydrogen bonded to a water molecule. Here, the same analysis is employed to observe interactions between the FPs and lipid headgroups.

3.2 Materials and Methods

3.2.1. Model Membrane Liposome Preparation

See Section 2.2.1 for DPPC lipid cake preparation procedure.

Instead of DPPC LUVs, DPPC small unilamellar vesicles (SUVs) were used in the equilibrium FTIR experiments. FTIR experiments require concentrated stock solutions of lipids since the total volume of each sample is only 40 uL, and LUVs are prone to aggregation at high concentrations due to their larger size. To prepare the SUVs, the

lipids were placed in a sonicator bath at 55° C for approximately 25 minutes, or until the cloudy lipid solution became visibly translucent. Vesicle size was confirmed via dynamic light scattering (DLS).

3.2.2. Fusion Peptide Preparation

See Section 2.2.2 for H3 fusion peptide preparation procedure.

3.2.3. FTIR

A Varian 660 FTIR spectrophotometer with a liquid N_2 cooled mercury cadmium telluride (MCT) detector was used to collect equilibrium FTIR data. In each experiment, the FP variant being studied was dissolved in D_2O and mixed with the DPPC SUVs in 20 mM sodium acetate deuterated buffer at pD 4.5. The FP was always present in concentration between 0.5 and 1 mM. The peptide to lipid ratios were 1:15 for WT, 1:30 for W14A, 1:50 for G8A, and 1:30 for G16A. A reference solution of 20 mM sodium acetate deuterated buffer at pD 4.5 with no FP or lipids was used.

A split IR cell with CaF_2 windows in a copper frame was used to hold the sample and reference solutions, which were separated by a 126 μM Teflon spacer. The mixture was kept cold to prevent the FP from inserting prior to initiating the experiment. After purging water vapor from the chamber, the sample was heated from 10° C to 50° C by 1° increments using a water bath. A thermocouple was used to monitor the actual temperature at the time of data collection. The following instrument parameters were used: 136 scans, 2 cm^{-1} resolution, total range of 15-6000 cm^{-1}. The final absorbance spectra were obtained by taking the negative logarithm of the ratio of the sample single beam spectrum to the reference at each temperature.

3.3 Results and Discussion

3.3.1 FTIR Peptide Amide Region

As temperature increases, helical peptides lose their helicity and become more disordered.[1] The broad decrease in signal from ~1610-1640 cm^{-1} represents loss of helical character.[1] The broad increase in signal from ~1640-1700 cm^{-1} represents the increase in disordered structure of the peptide at higher temperatures, with a dip at ~1670 cm^{-1} due to a TFA impurity.[1] In addition to these broad signal changes, it has been reported that the band at 1620 cm^{-1} corresponds to a solvated helix and the band around 1645 cm^{-1} corresponds to a helix in a hydrophobic environment.[1]

Figures 3.1 - 3.4 display the peptide amide regions of the FTIR spectra of each FP variant and DPPC SUVs heated from 10 to 50° C. The FTIR spectra for the G1V variant are not shown due to the presence of aggregation starting at low temperatures, most likely because the sample went bad. In each figure, the band at 1620 cm^{-1} decreases as the DPPC T_m is approached, indicating loss of solvated helix; at the same time, the band centered at 1645-1650 cm^{-1} grows, indicating the expected increase in buried helical character as each peptide variant inserts into the DPPC membrane. As temperature increases especially past the melting point, the feature centered around 1680 cm^{-1} increases, representing an increase in solvated disordered structure as the peptides unfold and become more shallowly inserted.[1] The features from 1700-1800 cm^{-1} shown in Figures 3.1 - 3.4 are from the lipid headgroup carbonyl stretch and are analyzed in section 3.3.3.

The magnitude of the increase in buried helix at 1620 cm^{-1} is greater than the magnitude of the decrease in solvated helix at 1645-1650 cm^{-1} for each FP, which likely

indicates that the peptides are folding within the membrane as they insert. This is supported by the observation from CD experiments (not shown here) that the FP requires the presence of lipid vesicles to fold into its α-helical conformation. It should also be noted that these graphs display equilibrium populations at each temperature.

There is no evidence of β-aggregation (which would appear as sharp positive peaks at 1620 and 1690 cm^{-1}) in these spectra, even at higher temperatures. According to the fluorescence emission data presented in section 2.3, the peptide must therefore be exiting the membrane or becoming solvated by water molecules leaking into the membrane.

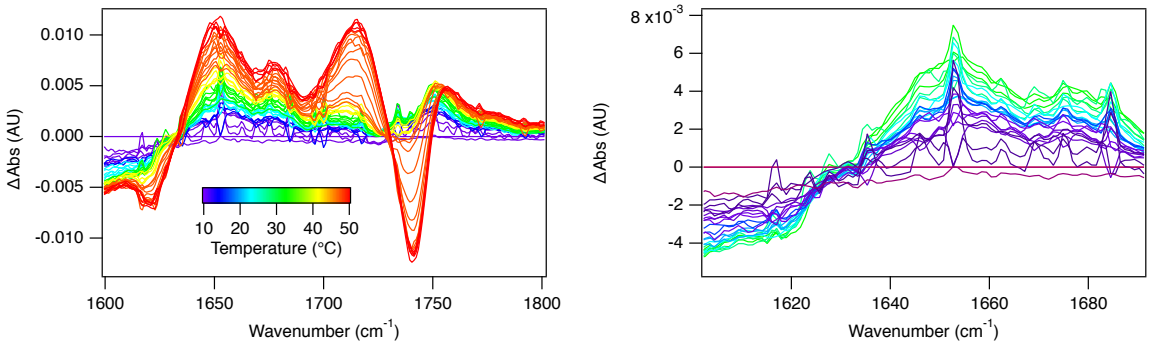

Figure 3.1. Peptide amide region of temperature-dependent FTIR emission difference spectra of WT FP and DPPC SUVs in a 1:15 molar ratio heated from 10° to 50° C. Difference spectra were calculated by subtracting the absorbance spectrum at 10° C from each subsequent temperature trace. The graph on the right shows only the difference spectra up to the melting point of DPPC (41° C) for clarity.

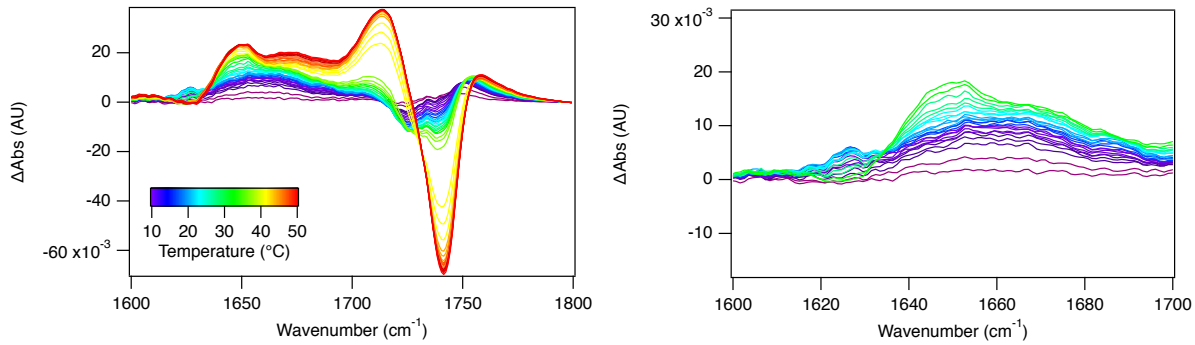

Figure 3.2. Peptide amide region of temperature-dependent FTIR emission difference spectra of W14A FP and DPPC SUVs in a 1:30 molar ratio heated from 10° to 50° C.

Unlike the other variants, the W14A FP displays an initial increase in solvated helical character along with the expected increase in buried helical character prior to the DPPC T_m (Figure 3.2). The W14A FP may be very shallowly inserting and folding as it interacts with the membrane. The subsequent decrease in solvated helical character approaching and beyond the DPPC T_m barely returns to baseline, also indicating that the W14A FP inserts shallowly compared to WT.

The positive buried helix bands shift from 1650 to 1645 cm^{-1} as temperature increases for the W14A, G8A, and G16A FPs (Figures 3.2 – 3. 4), which indicates that they are moving into a less hydrophobic environment, perhaps becoming less deeply inserted. This shift is not observed for the WT FP (Figure 3.1).

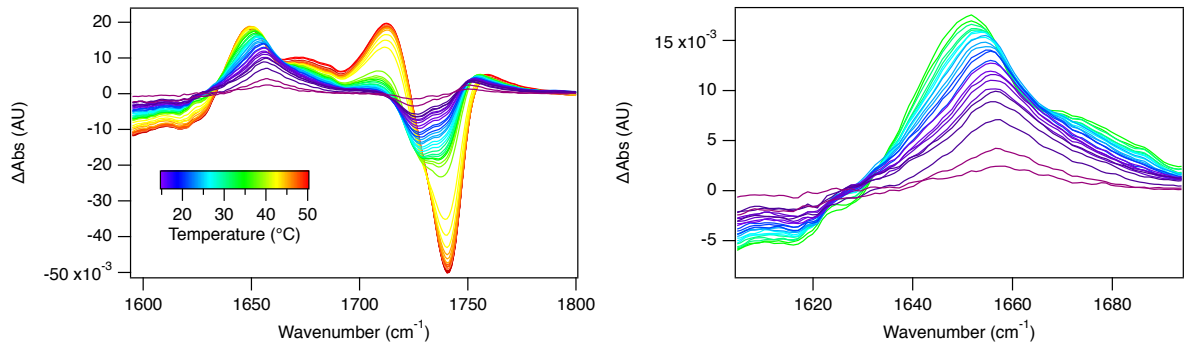

Figure 3.3. Peptide amide region of temperature-dependent FTIR emission difference spectra of G8A FP and DPPC SUVs in a 1:50 molar ratio heated from 10° to 50° C.

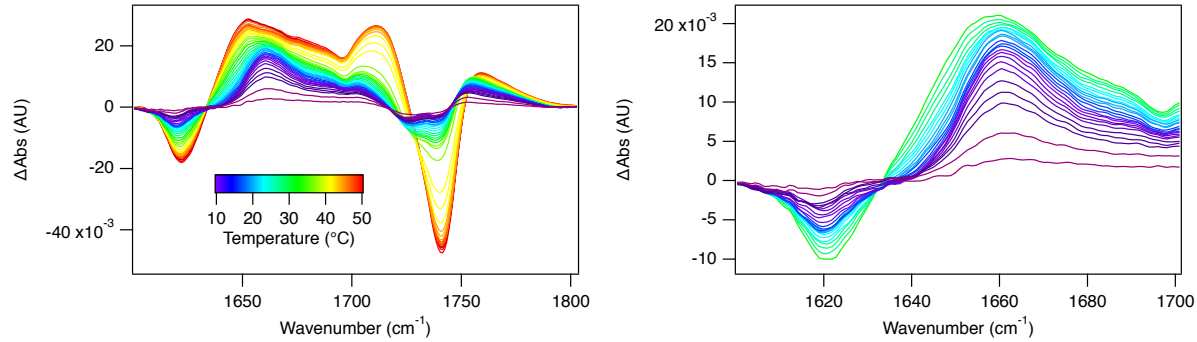

Figure 3.4. Peptide amide region of temperature-dependent FTIR emission difference spectra of G16A FP and DPPC SUVs in a 1:30 molar ratio heated from 10° to 50° C.

The G8A and G16A FPs (Figures 3.3 and 3.4) display increases in buried helix and decreases in solvated helix with a greater magnitude than WT. This observation is in agreement with the fluorescence data from Chapter 2 which showed that these variants inserted at lower temperatures and deeper than WT.

3.3.2 FTIR Lipid Tail CH Stretch Region

The symmetric and asymmetric CH stretches of the hydrophobic DPPC lipid tails appear at ~2850 and ~2920 cm^{-1}, respectively.[2] They display a broadening and shift to higher wavenumber as temperature increases due to higher conformational flexibility.[2] The rapid shift in peak intensity (which serves as a measure of peak broadening) and wavenumber of the CH stretch bands at 41° C represent the transition from the gel/ripple phase to the fluid phase, allowing FP insertion. These changes are shown for the WT FP in Figure 3.5.

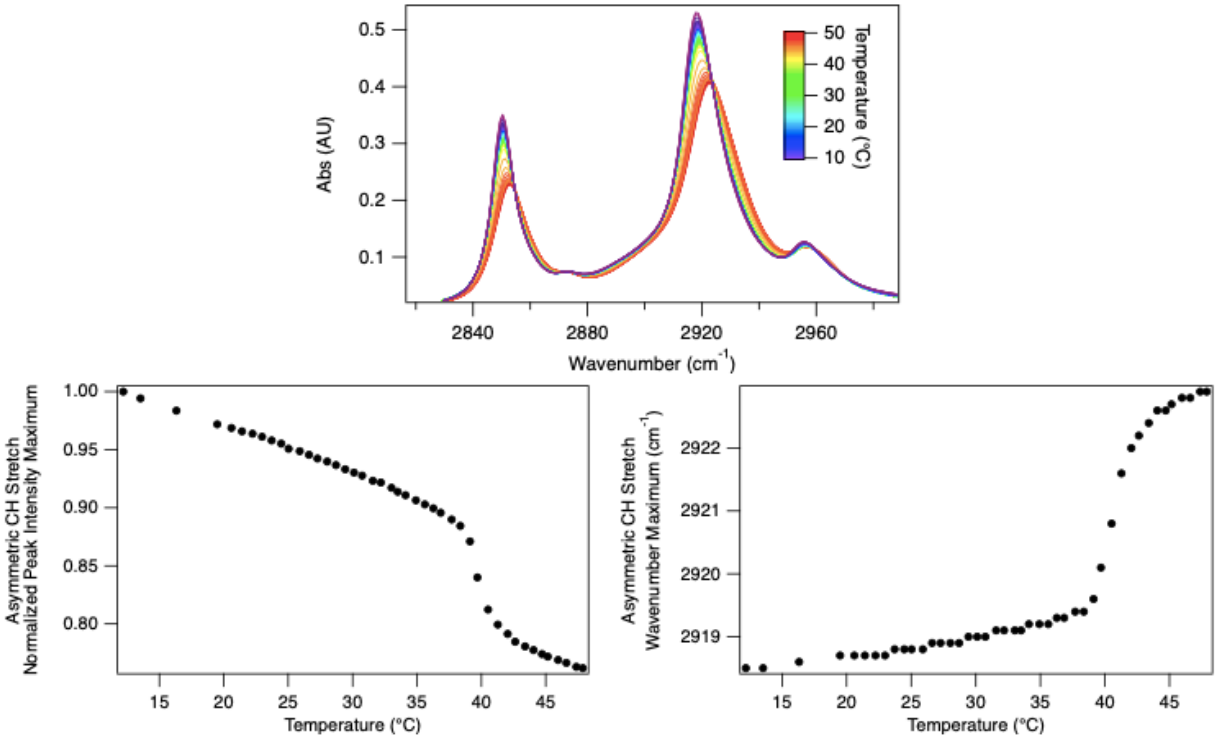

Figure 3.5. *Top*: Lipid hydrophobic tail region of temperature-dependent FTIR emission spectra of WT FP and DPPC SUVs in a 1:15 molar ratio heated from 10° to 50° C. The left peak represents the symmetric CH_2 stretch, the middle peak represents the asymmetric CH_2 stretch, and the small right peak represents the terminal CH_3 stretch.

Bottom left: Asymmetric CH stretch intensity maximum vs temperature. *Bottom right*: Asymmetric CH stretch wavelength maximum vs temperature.

Comparing the T_m shifts in peak intensity and wavenumber of the lipid tail CH stretches between different FP variants can reveal differences in insertion behavior. Figure 3.6 shows that the G8A and G16A variants cause peak broadening to the greatest extent, especially G16A. This indicates that they are disordering the lipid tails more than WT. In contrast, W14A disorders the lipid tails less than WT. These observations are consistent with the fluorescence data from Chapter 2 which provided evidence that the G8A and G16A variants insert deeper than the WT, while the W14A variant inserts more shallowly.

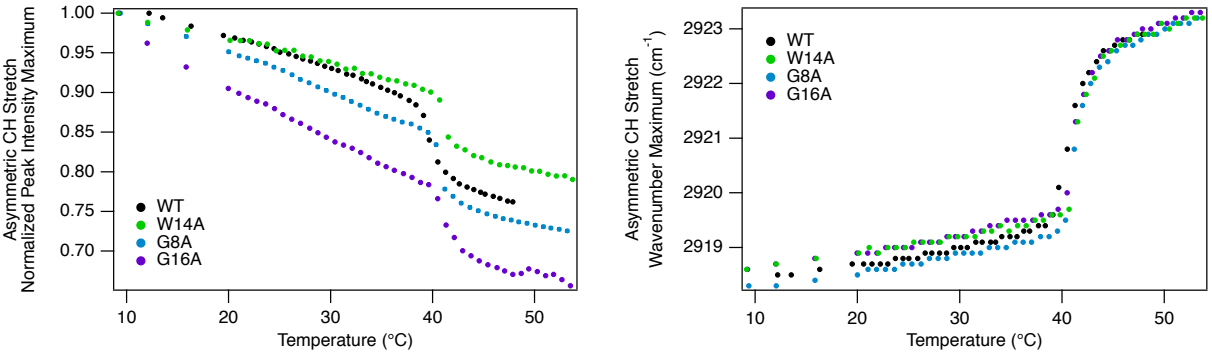

Figure 3.6. Lipid hydrophobic tail region of temperature-dependent FTIR emission spectra of WT, W14A, G8A, and G16A FPs and DPPC SUVs heated from 10° to 50° C. *Left*: Asymmetric CH stretch intensity maximum vs temperature for each FP variant. *Right*: Asymmetric CH stretch wavelength maximum vs temperature for each FP variant.

3.3.3 FTIR Lipid Headgroup Carbonyl Stretch Region

The phosphate ester carbonyl stretch appears from ~1700-1780 cm^{-1} and is composed of two overlapping bands: one centered at ~1730 cm^{-1} corresponding to a carbonyl with no H-bonds and the other at ~1745 cm^{-1} corresponding to a carbonyl with one H-bond.[3] The phosphate headgroups of DPPC are more water-accessible in the fluid phase, so the percent of H-bonded carbonyls increases at 41° C in the absence of FP. In the presence of FP, this expected behavior can be altered by changes in H-bonding between the phosphate headgroup carbonyls and the FP, as well as the influence of insertion on membrane surface structure.

The DPPC lipid headgroup carbonyl regions of the FTIR melt spectra for each FP variant are shown in Figure 3.7. For each variant except WT, there is a visible shift of this peak to lower wavenumbers near the DPPC T_m. These shifts are shown quantitatively in Figure 3.9.

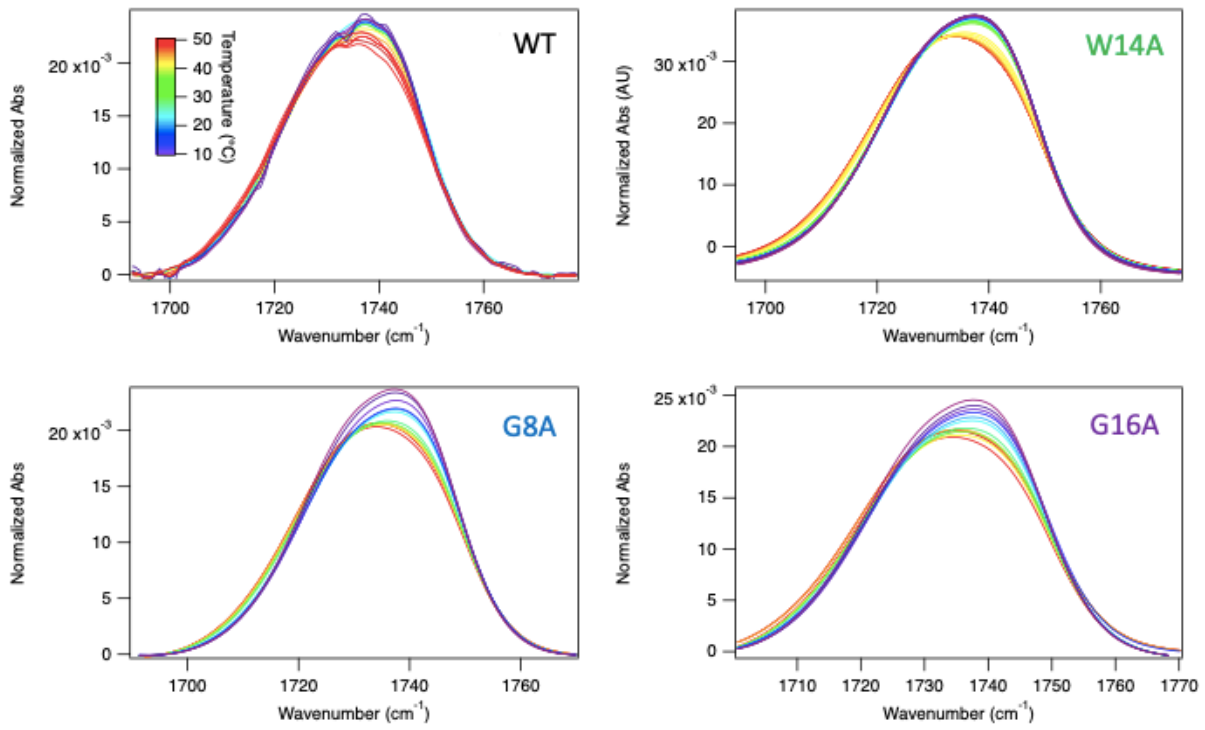

Figure 3.7. Lipid phosphate headgroup ester regions of temperature-dependent FTIR emission spectra of WT, G8A, and G16A FPs and DPPC SUVs heated from 10° to 50° C.

Figure 3.8 displays the DPPC headgroup carbonyl band at different temperatures for the WT FP, fit to a double gaussian and broken up into its component H-bonded and non-H-bonded bands in order to calculate the percent of H-bonded carbonyls.

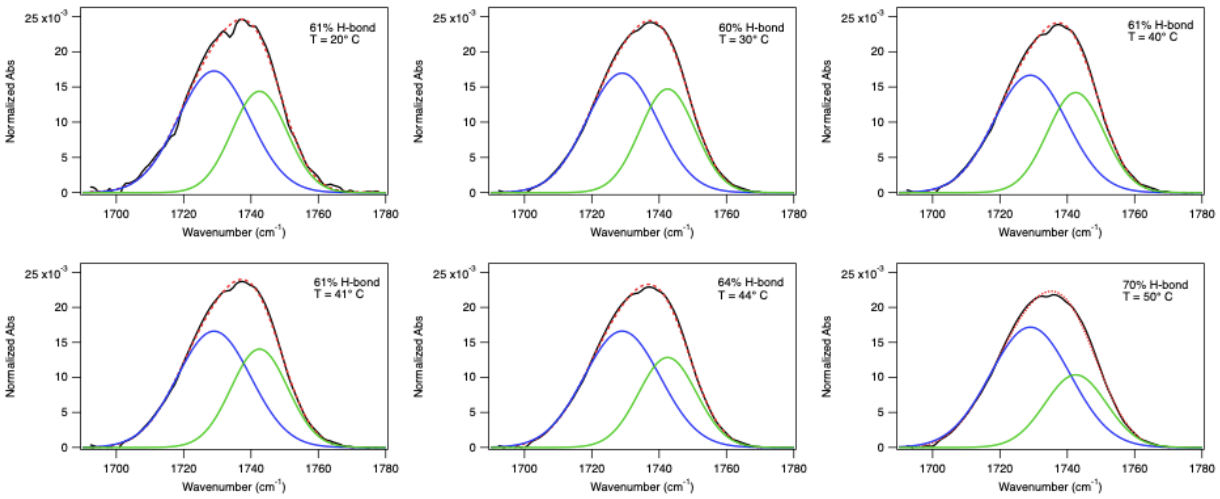

Figure 3.8. Lipid phosphate headgroup ester region of temperature-dependent FTIR emission spectra of WT FP and DPPC SUVs in a 1:15 molar ratio heated from 10° to 50° C. The peak was fit to a double gaussian, with the lower-wavelength gaussian representing esters with one H-bond and the higher-wavelength gaussian representing non-H-bonded esters. The percent of H-bonded esters was calculated by taking the ratio of the integrals of the H-bonded peak and the total combined peak.

The differences in calculated DPPC headgroup carbonyl H-bonding for each FP variant are shown in Figure 3.9. As visible in Figure 3.7, the WT FP displays a more gradual increase in carbonyl H-bonding shown by its shallower slope, which also occurs at higher temperatures compared to the variants. Since the FP variants display the expected shift in carbonyl H-bonding at the DPPC T_m and the WT FP does not, the WT FP may have the strongest interaction with the DPPC headgroups.

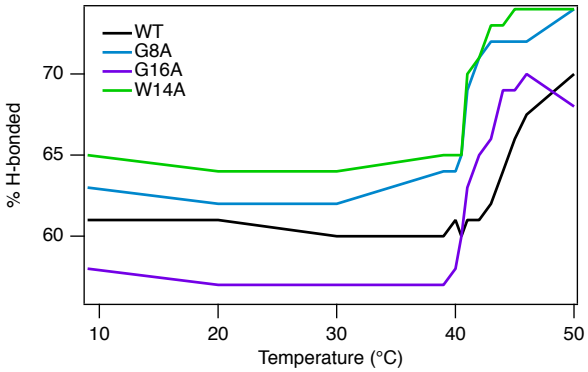

Figure 3.9. Percent H-bonded carbonyls of DPPC headgroups during FTIR melts of WT, G8A, and G16A FPs and DPPC SUVs. Calculated by resolving the phosphate headgroup ester band between 1680-1780 cm^{-1} into its component H-bonded and non-H-bonded bands.

Although Figure 3.9 shows the DPPC headgroups beginning at different percent H-bonded values in the presence of each variant, this may be a result of systematic error in the calculations.

3.3.4 FTIR Reversibility Experiment

The reversibility of FP insertion was studied using FTIR spectroscopy by cooling the mixture of DPPC SUVs and WT FP from 50° to 20° C (Figure 3.10). Similar to the results of the fluorescence study from Chapter 2, FP insertion appears mostly irreversible. The peptide amide region shows only a slight shift back to baseline. There is still a positive buried helix feature and a negative solvated helix feature after cooling back to 20° C, indicating that the FP is still mostly inserted in the membrane. However, the lipid tail CH stretches return back to baseline, indicating that the FP is no longer inserted in the membrane deeply enough to disorder the lipid tails. The amide region of

the FTIR spectra indicated that the FPs become more shallowly inserted and disordered at higher temperatures, which appears to be an irreversible process.

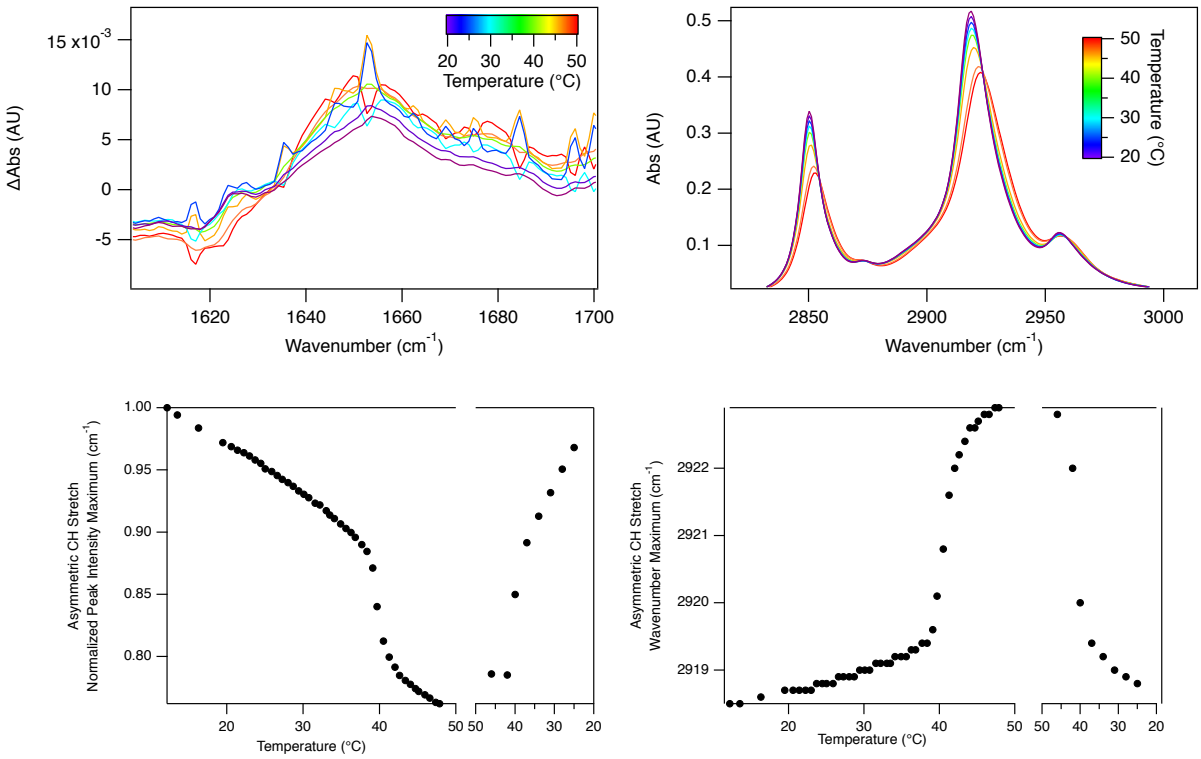

Figure 3.10. Temperature-dependent FTIR spectra of WT FP and DPPC SUVs in a 1:15 molar ratio cooled from 50° to 20° C. *Top left:* Peptide amide region of FTIR spectra. *Top right:* Lipid tail CH stretch region of FTIR spectra. *Bottom left*: Asymmetric CH stretch intensity maximum vs temperature. *Bottom right*: Asymmetric CH stretch wavelength maximum vs temperature.

3.4 References

1. Brewer, S. H.; Tang, Y.; Vu, D. M.; Gnanakaran, S.; Raleigh, D. P.; Dyer, R. B. Temperature Dependence of Water Interactions with the Amide Carbonyls of α-Helices. *Biochemistry* **2012**, *51* (26), 5293–5299.

2. Lewis, R. N. A. H.; McElhaney, R. N. Membrane Lipid Phase Transitions and Phase Organization Studied by Fourier Transform Infrared Spectroscopy. *Biochimica et Biophysica Acta (BBA) - Biomembranes* **2013**, *1828* (10), 2347–2358.
3. Valentine, M. L.; Waterland, M. K.; Fathizadeh, A.; Elber, R.; Baiz, C. R. Interfacial Dynamics in Lipid Membranes: The Effects of Headgroup Structures. *The Journal of Physical Chemistry B* **2021**, *125* (5), 1343–1350.

Chapter 4: Conclusions and Perspectives

4.1 Conclusions and Perspectives

Influenza hemagglutinin plays a crucial role in viral infection by driving fusion between the viral and host cell endosomal membranes. The fusion peptide, a highly conserved region of HA essential for this fusion process, has proven difficult to study structurally due to its hydrophobic nature. The dynamics of its insertion and how it drives membrane fusion remain uncertain. Fluorescence and FTIR spectroscopy are ideally suited for studying FP interactions with membranes because they can probe changes in environment around specific groups on both the FP and the membrane lipids.

The insertion behavior of different FP variants into model membranes has been investigated using temperature-dependent intrinsic tryptophan fluorescence emission and FTIR spectroscopy. Since both techniques showed FP insertion to be irreversible, it cannot consist of a simple two-state process. In reality, at least four steps are visible in the equilibrium data presented in Chapters 2 and 3: beginning at low temperatures, the FPs associate with the DPPC vesicle membrane surface; as temperature increases below the DPPC T_m, FPs in the open conformation can insert into the membrane defects present during the ripple phase; at the T_m, when the membrane transitions into the fluid phase, FPs in the open conformation can insert to a greater extent and possibly deeper into the fluid membrane; and finally, as temperature increases above the T_m, FP insertion becomes shallower, and the FPs and membrane environment become more disordered.

Together, fluorescence and FTIR spectroscopy provide cohesive information about the effect of FP structure on insertion behavior. The G1V and W14A variants, which

adopt linear and wide-angle bent structures respectively,[1,2] insert more shallowly or allow more water leakage into the membrane than the WT FP. Although wider-angle conformations are likely important for spanning the endosomal membrane during the later steps in membrane fusion (fusion pore formation), it appears that they are disruptive during the early steps (insertion and hemifusion). This would explain why both the G1V and W14A FP variants have reportedly failed to drive both hemifusion and full fusion.[3] The G8A and G16A variants, which can adopt acute angle open conformations,[4] insert at lower temperatures and disorder the lipid tails more than WT. The acute angle open conformation therefore seems to be important for insertion and strong membrane interaction. Since the G8A FP has reportedly failed to drive both hemifusion and full fusion,[3] it is possible that the closed helical hairpin conformation is important for hemifusion.

Immediate next steps should be to perform lipid and contents mixing assays to determine if any of the FP variants are driving hemifusion or fusion apart from the rest of the HA protein. This would aid in interpreting the fluorescence and FTIR melt data in Chapters 2 and 3.

With the equilibrium temperature-dependent fluorescence emission and FTIR absorbance spectra established, kinetics experiments can be performed to determine the timescale of FP insertion into model membrane vesicles. Time-resolved temperature-jump fluorescence and FTIR spectroscopy experiments should be performed to accomplish this. Kinetics experiments will be important in studying the dynamics of fusion peptide insertion that cannot be studied under equilibrium conditions. Probing these dynamics and how they drive membrane fusion is critical for

understanding the overall mechanism of membrane fusion, a process that is relevant to viral infection and many other cellular processes.

4.2 References

1. Li, Y.; Han, X.; Lai, A. L.; Bushweller, J. H.; Cafiso, D. S.; Tamm, L. K. Membrane Structures of the Hemifusion-Inducing Fusion Peptide Mutant G1S and the Fusion-Blocking Mutant G1V of Influenza Virus Hemagglutinin suggest a Mechanism for Pore Opening in Membrane fusion. *Journal of Virology* **2005**, *79* (18), 12065–12076.
2. Lai, A. L.; Park, H.; White, J. M.; Tamm, L. K. Fusion Peptide of Influenza Hemagglutinin Requires a Fixed Angle Boomerang Structure for Activity. *Journal of Biological Chemistry* **2006**, *281* (9), 5760–5770.
3. Cross, K.; Langley, W.; Russell, R.; Skehel, J.; Steinhauer, D. Composition and Functions of the Influenza Fusion Peptide. *Protein & Peptide Letters* **2009**, *16* (7), 766–778.
4. Lorieau, J. L.; Louis, J. M.; Schwieters, C. D.; Bax, A. PH-Triggered, Activated-State Conformations of the Influenza Hemagglutinin Fusion Peptide Revealed by NMR. *Proceedings of the National Academy of Sciences* **2012**, *109* (49), 19994–19999.